

# Securing Time in Energy IoT: A Clock-Dynamics-Aware Spatio-Temporal Graph Attention Network for Clock Drift Attacks and Y2K38 Failures

Saeid Jamshidi, Omar Abdul-Wahab, Rolando Herrero, and Foutse Khomh

**Abstract**—The integrity of time across distributed Internet of Things (IoT) devices is fundamental to reliable sensing, control, and security in *energy cyber-physical systems*, including smart grids, microgrids, and distributed energy management platforms. However, operational energy IoT systems remain vulnerable to clock drift escalation, time-synchronization manipulation, and catastrophic timestamp discontinuities such as the Year 2038 (Y2K38) Unix epoch overflow, all of which violate timestamp monotonicity and distort temporal ordering in system observations. These timing-layer failures induce structured temporal inconsistencies that conventional anomaly detection models, which implicitly assume reliable timestamps, are ill-equipped to capture. This paper introduces STGAT (Spatio-Temporal Graph Attention Network), a clock-dynamics-aware anomaly detection framework that jointly models temporal distortion and inter-device consistency in energy IoT systems. STGAT combines drift-aware temporal embeddings with temporal self-attention to capture non-uniform and corrupted time evolution at individual devices, and graph attention to model the spatial propagation of timing inconsistencies across interconnected nodes. A curvature-regularized latent representation is further employed to geometrically separate nominal clock evolution from anomalous temporal deformation arising from drift escalation, synchronization offsets, and epoch-overflow events. An experimental evaluation of energy IoT telemetry augmented with controlled timing-layer perturbations demonstrates that STGAT achieves 95.7% accuracy, consistently outperforming recurrent, transformer-based, and graph-based baselines with statistically significant improvements and large effect sizes ( $d > 1.8$ ,  $p < 0.001$ ). Moreover, STGAT reduces detection delay to 2.3 time steps, corresponding to a 26% improvement over the closest baseline, while maintaining stable performance under overflow-induced discontinuities, stealthy drift escalation, and temporally induced physical inconsistencies.

**Index Terms**—Internet of Things (IoT), Time Synchronization, Y2K38, Timestamp Drift, NTP Spoofing, GPS Spoofing, Temporal Anomaly Detection, Spatio-Temporal Graph Attention Network (STGAT)

## I. INTRODUCTION

The integration of Internet-of-Things (IoT) devices into modern energy cyber-physical systems, including smart grids,

Corresponding author: Saeid Jamshidi (saeid.jamshidi@polymtl.ca).

Saeid Jamshidi and Omar Abdul-Wahab are with the Department of Computer and Software Engineering, Polytechnique Montréal, Québec, Canada.

Foutse Khomh is with the SWAT Laboratory, Polytechnique Montréal, Québec, Canada.

Rolando Herrero is with the College of Engineering, Northeastern University, Boston, MA, USA (email: r.herrero@northeastern.edu).

microgrids, distributed energy resources, and electric vehicle charging infrastructures, has fundamentally transformed monitoring, protection, and control paradigms [1], [2], [3]. These systems operate as tightly coupled spatio-temporal processes in which sensing, actuation, and control decisions depend on the correct ordering and alignment of distributed timestamps. Consequently, *temporal integrity*, the correctness, monotonicity, and cross-device consistency of time, constitutes a core system invariant rather than a mere implementation detail. Violations of temporal integrity distort causality, destabilize control loops, and compromise both operational safety and forensic reliability [4], [5].

Maintaining reliable temporal integrity in energy IoT systems is inherently challenging. Embedded devices rely on low-cost oscillators that exhibit frequency drift due to environmental variability, aging, and manufacturing tolerances [6]. Time synchronization mechanisms such as NTP, PTP, and GNSS-based timing introduce latency, jitter, and correction noise, leading to gradual temporal deformation that accumulates over long operational horizons [7]. Importantly, such deformation does not merely add noise to timestamps; it alters the effective temporal sampling process, reshapes the geometry of time-indexed data streams, and violates the implicit assumption of consistent temporal ordering underpinning many learning-based monitoring and anomaly detection methods.

A particularly critical yet underexplored class of temporal failure arises from catastrophic timestamp discontinuities, exemplified by the *Year 2038 Unix Epoch Overflow* (Y2K38) [8]. Many long-lifecycle embedded and industrial IoT devices continue to rely on 32-bit signed Unix time representations due to firmware inertia, legacy operating systems, certification constraints, and limited update paths [9], [10]. When such devices exceed the maximum representable timestamp on January 19, 2038, counter wraparound induces an abrupt loss of temporal monotonicity [11], [12], [13]. From a signal-processing perspective, this event constitutes a singular temporal discontinuity whose magnitude exceeds ordinary drift and jitter by several orders of magnitude. More broadly, Y2K38 is a concrete instance of a class of epoch-related failures that can occur when finite timestamp representations overflow. Beyond benign failures, adversaries can deliberately manipulate time through timing-layer attacks such as NTP spoofing and GPS/GNSS time-reference manipulation, injecting controlled offsets and slow drift to evade detection while

gradually desynchronizing devices [14], [15]. Both natural and adversarial timing faults, therefore, undermine the foundational assumption of reliable temporal ordering in energy IoT systems.

Despite these risks, existing anomaly detection approaches remain poorly equipped to reason explicitly about temporal integrity. Sequence-based models such as LSTM and GRU architectures treat timestamps as reliable indices and focus on learning correlations in signal values, implicitly assuming uniform and mildly irregular sampling [16], [17]. Graph-based and spatio-temporal graph neural networks capture spatial dependencies among devices but typically assume consistent temporal alignment across nodes, limiting their sensitivity to clock drift, synchronization faults, and timestamp discontinuities [18], [19]. More generally, time corruption is rarely modeled as a first-class phenomenon governed by clock dynamics, offset corrections, jitter accumulation, and overflow events. As a result, timing-layer failures often remain latent until they propagate into higher-level physical or operational anomalies. This paper addresses this gap by introducing *STGAT* (Spatio-Temporal Graph Attention Network), a clock-dynamics-aware learning framework for detecting *timing-layer failures* in energy IoT systems. Device-reported time is modeled as a deformable temporal signal governed by stochastic clock drift, synchronization offsets, jitter accumulation, and epoch-overflow events, and these dynamics are embedded directly into the learning process through drift-aware temporal embeddings. STGAT combines *temporal self-attention*, which captures non-uniform and corrupted time evolution within individual device streams, with *graph attention*, which models the spatial propagation and cross-device consistency of temporal distortions across interconnected nodes. To distinguish benign clock evolution from anomalous temporal behavior, a curvature-regularized objective promotes geometric separation between nominal and corrupted temporal trajectories in the latent representation space. An online sequential detection mechanism further enables early identification of timing anomalies before temporal faults propagate into observable physical and operational inconsistencies. The main contributions of this work are summarized as follows:

- 1) **Temporal integrity modeling for energy IoT:** We formalize timing-layer failure modes, including clock drift escalation, synchronization offset shocks, jitter accumulation, and epoch-overflow events, as deformations acting on temporal manifolds.
- 2) **Curvature-aware spatio-temporal graph learning:** We propose STGAT, a clock-dynamics-aware spatio-temporal graph attention architecture that jointly models temporal deformation and inter-device dependencies through drift-aware embeddings, temporal self-attention, graph attention, and curvature-regularized latent geometry.
- 3) **Empirical evaluation under timing failures:** We evaluate STGAT under diverse timing-layer failure scenarios and demonstrate improved detection accuracy, reduced detection latency, and statistically significant robustness compared to representative temporal, graph-based, and hybrid baselines.

The remainder of this paper is organized as follows. Section II reviews previous work on time synchronization in energy and industrial IoT systems, time-synchronization attacks, and deep spatio-temporal anomaly detection models. Section III presents the proposed STGAT solution, including the physics-aware temporal operators, drift-aware embeddings, spatio-temporal graph attention mechanisms, and curvature-regularized optimization. Section V reports the experimental evaluation, covering overall detection performance, detection delay, temporal and physical feature analysis, latent geometry characterization, comparison with Previous spatio-temporal detectors, and component contribution analysis. Section VI discusses the implications of the results and their relevance to temporal integrity and Y2K38 resilience in energy IoT systems. Section VII outlines the limitations of the proposed approach and directions for future research. Section VIII concludes the paper.

## II. RELATED WORK

This section reviews three research directions closely related to the proposed STGAT solution: 1) time synchronization in smart grids and industrial IoT, 2) time-synchronization attacks and spoofing-resilient protection mechanisms, and 3) deep spatio-temporal models for multivariate time-series anomaly detection.

### A. Time Synchronization in Smart Grids and Industrial IoT

Accurate and stable time synchronization is a foundational requirement for large-scale IoT systems and energy cyber-physical systems. Yigitler et al. survey synchronization techniques for IoT systems, highlighting trade-offs among accuracy, energy consumption, and hardware complexity in heterogeneous wireless networks [20]. Liu et al. provide a review of clock synchronization in the Industrial Internet, addressing protocol-level mechanisms, oscillator behavior, and cross-layer co-design challenges for delay-sensitive applications [21]. More recently, Liu et al. focus on modern smart grids, discussing stringent timing requirements for phasor measurement units (PMUs), protection relays, and advanced metering infrastructure, and emphasizing the growing reliance on GNSS- and PTP-based timing in distributed energy systems [22]. These studies collectively underscore the criticality of time accuracy but largely assume that synchronization mechanisms operate under nominal conditions.

### B. Time-Synchronization Attacks and Spoofing Countermeasures

A substantial body of work investigates adversarial manipulation of time references, particularly through GNSS/GPS spoofing and related attacks. Zhang et al. analyze GPS spoofing-based time-synchronization attacks in power systems, demonstrating how falsified timing signals can desynchronize monitoring and control operations, and reviewing hardware and signal-processing-based countermeasures [23]. Xue et al. propose a data-driven spoofing detection method leveraging PMU measurements to identify and correct phase-angle

distortions [24]. Khan et al. introduce an incremental GPS spoofing strategy that injects low-rate perturbations into PMU time series, showing that such attacks can evade conventional detection schemes [25].

More recent studies apply Deep Learning (DL) to timing attacks. Liu et al. develop an LSTM-based detection and mitigation framework for time-synchronization attacks under GNSS spoofing [26], while Sabouri et al. combine recurrent models for both detection and correction of spoofed measurements in power networks [27]. Ou et al. propose a protection scheme that integrates multi-source measurements and signal-level validation to improve resilience against GNSS spoofing and jamming [28]. Although effective in specific scenarios, these approaches primarily focus on attack detection and measurement level and do not model time corruption as a continuous, system-wide temporal deformation process.

### C. Deep and Spatio-Temporal Graph Models for Time-Series Anomaly Detection

DL has become the dominant paradigm for detecting anomalies in multivariate time series in industrial and IoT systems. Jia et al. survey deep anomaly detection methods, categorizing architectures such as autoencoders, recurrent networks, transformers, and generative models, and emphasizing the importance of capturing long-range temporal dependencies [29]. Backhus et al. propose a hybrid signal-processing and DL pipeline, demonstrating improved robustness on industrial telemetry [30]. Transformer-based methods, such as RTdetector, leverage global attention and reconstruction trends to detect complex temporal anomalies [31].

Beyond purely temporal models, spatio-temporal graph neural networks (STGNNs) have been proposed to capture dependencies among interconnected variables or devices. Zheng et al. introduce GST-Pro, which models multivariate time series using graph-based controlled differential equations and distributional anomaly scoring [32]. Di et al. design an interpretable GNN for satellite power-system anomaly detection, emphasizing relational modeling and explainability [33]. In industrial IoT settings, Lu et al. demonstrate that spatio-temporal GNNs improve anomaly detection by fusing network, process, and sensor data [34]. AlZahrani et al. address real-time anomaly detection in IoT data streams, highlighting challenges related to streaming constraints, concept drift, and resource efficiency [35].

Existing spatio-temporal graph neural networks and transformer-based anomaly detection models effectively capture temporal and spatial dependencies when timestamps are reliable, but they typically omit explicit modeling of clock drift, synchronization offsets, jitter accumulation, and epoch-overflow events. Although irregular-time transformers, time-aware recurrent models, and event-based approaches handle non-uniform sampling, they generally treat timestamp irregularity as a sampling artifact and continue to assume semantically valid, monotonically ordered time. In contrast, the proposed *STGAT* framework treats time corruption as a first-class phenomenon by modeling device-reported timestamps as

deformable entities governed by clock dynamics and overflow behavior. By embedding clock-aware temporal features and leveraging graph attention to capture the spatial propagation of timing inconsistencies, STGAT enables principled detection of timing-layer failures, including Y2K38-related disruptions, that cannot be reliably identified by methods assuming timestamp integrity.

## III. PROPOSED MODEL

This section presents STGAT, a curvature-aware spatio-temporal graph attention network for detecting *timing-layer failures* in energy IoT systems. The proposed model is grounded in a *physics-informed temporal modeling* solution that explicitly captures the physical behavior of device clocks, treating reported timestamps as deformable signals impacted by clock drift, synchronization offsets, jitter accumulation, and epoch-overflow events. Rather than assuming reliable temporal ordering, STGAT embeds timing distortions directly into the learning process via operator-level formulations, enabling principled reasoning about temporal integrity at the timestamp level. At its core, STGAT integrates drift-aware temporal embeddings with transformer-based temporal attention and multi-head graph attention. The temporal component models non-uniform sampling and clock evolution induced by oscillator drift and synchronization disturbances, while the graph-attention component captures the spatial propagation of temporal inconsistencies across interconnected IoT devices. This joint spatio-temporal modeling allows STGAT to simultaneously learn device-level temporal anomalies and network-level correlation patterns, which is essential for detecting both gradual drift escalation and abrupt Y2K38-induced timestamp discontinuities in energy IoT networks.

Figure 1 illustrates the end-to-end STGAT pipeline. Input multivariate time series are first preprocessed and augmented with drift-aware temporal features, then passed through a temporal encoder that incorporates transformer-based self-attention with drift-and overflow-aware embeddings. The resulting representations are fused via spatial graph attention to model inter-device dependencies, followed by a curvature-regularized optimization and decision layer. The feedback paths in the architecture illustrate how timestamp distortions propagate across both temporal and spatial dimensions, linking operator-level temporal deformation to network-level anomaly detection. To provide a theoretical foundation, we formalize a set of temporal operators governing timestamp distortion and analyze their impact on the latent representation space. Moreover, these operators characterize how clock drift, offset jumps, jitter, and epoch-overflow events deform the effective temporal sampling process, inducing measurable geometric curvature in the learned temporal manifold. By explicitly modeling these deformation mechanisms, STGAT distinguishes benign clock evolution from adversarial and catastrophic timing failures without relying on downstream physical anomalies. The resulting operator-level definitions directly inform the construction of drift-aware embeddings, attention mechanisms, curvature regularization terms, and online detection logic, ensuring that STGAT remains temporally grounded, overflow-aware, and

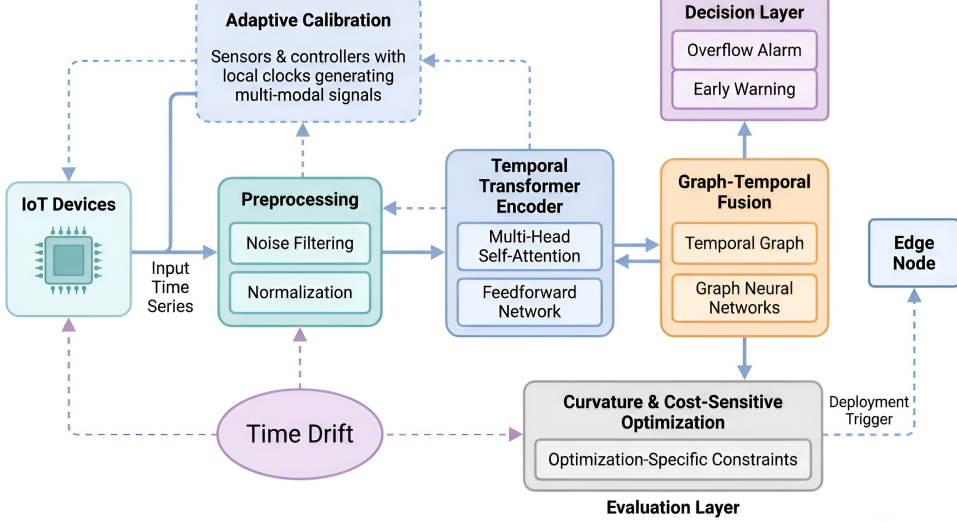


Fig. 1: Overview of the proposed STGAT architecture.

robust against real-world timestamp integrity violations in energy IoT systems.

#### A. System Operators and Distortion Modeling

Each device  $v_i$  produces a multivariate measurement stream:

$$\mathbf{x}_i(t) \in \mathbb{R}^{F_s}, \quad t \in \{1, \dots, T\},$$

where  $F_s$  denotes the number of sensing modalities (e.g., voltage, current, frequency, and thermal measurements). We assume that all devices observe the underlying physical process synchronously in real time, but *report* their measurements asynchronously due to clock drift, synchronization offsets, and potential epoch-overflow events. Importantly, temporal distortion affects the *timestamp layer* rather than the physical sensing process itself.

*Timestamp Operator:* Consider an energy IoT system composed of  $N$  devices, indexed by  $i \in \{1, \dots, N\}$ . Each device  $v_i$  maintains a local notion of time modeled as:

$$\tau_i(t) = t + \delta_i(t) + \eta_i(t) + o_i(t) T_0.$$

This operator decomposes the device-reported timestamp into four components:

- $t$ : the true global physical time shared across all devices.
- $\delta_i(t)$ : a continuous drift function (phase deviation), typically modeled as a stochastic process, capturing the cumulative frequency mismatch between the local oscillator of device  $v_i$  and the global clock.
- $\eta_i(t)$ : a discrete offset term representing abrupt time adjustments caused by GPS and NTP synchronization events, as well as manual corrections applied at device  $v_i$ .
- $o_i(t) T_0$ : an overflow operator activated when the internal 32-bit signed Unix timestamp counter of device  $v_i$  exceeds  $T_0 = 2^{31}$ , explicitly encoding the Year 2038 (Y2K38) rollover.

The inclusion of the overflow term  $o_i(t)$  is critical: once a rollover occurs, timestamps wrap into the negative interval

$[-2^{31}, -1]$ , inducing a loss of temporal monotonicity. Our formulation is deliberately agnostic to firmware-specific implementation details and hardware platforms, and instead models overflow as a device-local temporal discontinuity of fixed magnitude  $T_0$ .

*Distortion Operator:* We isolate temporal distortion as:

$$\Psi_i(t) = \tau_i(t) - t, \quad \Delta\Psi_i(t) = \Psi_i(t + \Delta t) - \Psi_i(t).$$

Here,

- $\Psi_i(t)$  captures the absolute deviation between local device time and true physical time.
- $\Delta\Psi_i(t)$  quantifies the *incremental distortion*, which is central to anomaly detection because it encodes whether the device clock advances faster and slower than the physical process.

Under nominal conditions,  $\Delta\Psi_i(t) \approx 0$ . In contrast, drift escalation, spoofing-induced offset shocks, and Y2K38 rollover events produce pronounced deviations, with epoch overflow introducing a catastrophic discontinuity of magnitude  $T_0$ .

*Distorted Sampling Operator:* We define a drift-aware sampling operator:

$$(\mathcal{S}_i \mathbf{x})(t) = \mathbf{x}(t + \Psi_i(t)),$$

which reflects the fact that devices sense the physical world at the correct physical time, while the *timestamps associated with the recorded samples* are distorted. As a result, the dataset is indexed by the corrupted time  $\tau$  rather than the true time  $t$ . From the perspective of the learning algorithm, the observed data lie on a warped temporal manifold:

$$\mathcal{M}_i = \{(t, \mathbf{x}_i(t)) \mapsto (\tau_i(t), \mathbf{x}_i(t))\}.$$

This temporal warping is fundamental to anomaly detection: misaligned timestamps introduce false causality, cause identical events across devices to appear at different temporal indices, and lead attention-based architectures to compute correlations over inconsistent time references. Y2K38 rollover injects an extreme discontinuity of magnitude  $T_0$ , which

can severely destabilize temporal reasoning unless explicitly modeled. This operator-level formulation enables principled discrimination among benign clock drift, synchronization-induced offset jumps, overflow-driven discontinuities, and intentional violations of temporal monotonicity. The remainder of the proposed methodology builds directly upon these operators, constructing drift-aware temporal embeddings, spatio-temporal inference mechanisms, and curvature-sensitive optimization strategies that keep STGAT robust under severe timestamp distortions, including Y2K38 rollover events.

### B. Algorithm 1: Drift-Aware Dataset Construction

Algorithm 1 generates a physically grounded dataset that exposes the model to a range of temporal failure modes observed in energy IoT systems, including oscillator drift, synchronization offset jumps, desynchronization shocks, adversarial timestamp perturbations, and the Y2K38 epoch overflow. Rather than acting as a simple data-augmentation routine, the algorithm explicitly simulates device-level time deformation and constructs warped temporal manifolds that are subsequently used to train the proposed STGAT architecture. The drift evolution:

$$\delta_{i,t} = \alpha_i \delta_{i,t-1} + \sigma_i \sqrt{\Delta t} \epsilon_t$$

corresponds to the Euler-Maruyama [36] discretization of an Ornstein-Uhlenbeck [37] process, which models oscillator-induced timestamp divergence. Synchronization offset dynamics:

$$\eta_{i,t} = \eta_{i,t-1} + \xi_t$$

capture abrupt time adjustments arising from NTP corrections, pulse-per-second (PPS) glitches, and jitter. The overflow operator:

$$o_{i,t} = \mathbb{I}(\tau_{i,t-1} \geq T_0), \quad T_0 = 2^{31},$$

injects the catastrophic Y2K38-induced discontinuity into the timestamp sequence. The resulting timestamp composition:

$$\tau_{i,t} = t + \delta_{i,t} + \eta_{i,t} + o_{i,t} T_0, \quad \Psi_i(t) = \tau_{i,t} - t,$$

defines the distorted local time base for device  $v_i$ . Temporal irregularities are encoded through the time-drift embedding vector:

$$\mathbf{d}_t = [\Delta t_t, \delta_t, \eta_t, o_t]^\top,$$

which is injected into the warped feature representation:

$$\mathbf{z}_t = \mathbf{x}_t + W_t \mathbf{d}_t.$$

This embedding induces curvature in the latent temporal manifold, quantified as:

$$K(t) = \|J(t)^\top J(t) - I\|_F.$$

Each tuple  $(\mathbf{z}_t, \Psi_i(t), K(t))$  therefore captures the warped signal representation, the underlying timestamp distortion, and the local manifold geometry, forming a compact yet expressive characterization of temporal corruption patterns essential for training Y2K38-aware detection models. Algorithm 1 yields a differentiable and physically grounded representation of timestamp corruption encompassing drift accumulation, syn-

chronization offsets, and Y2K38 epoch overflow. The overflow term  $o_{i,t} T_0$  introduces a discontinuity several orders of magnitude larger than ordinary drift and jitter, imprinting a distinctive geometric signature on the latent manifold. By directly embedding these distortions into the training data, STGAT learns to recognize timing-layer failures across heterogeneous devices and synchronization conditions, thereby forming a robust foundation for detecting real-world Y2K38-related temporal faults.

---

### Algorithm 1 Drift-Aware Data Construction

---

```

1:  $\mathcal{D} \leftarrow \emptyset$ 
2: for  $i = 1$  to  $N$  do
3:   Initialize  $\delta_{i,0}, \eta_{i,0}, o_{i,0} \leftarrow 0$ 
4:   for  $t = 1$  to  $T$  do
5:      $\delta_{i,t} \leftarrow \alpha_i \delta_{i,t-1} + \sigma_i \sqrt{\Delta t} \epsilon_t$ 
6:      $\eta_{i,t} \leftarrow \eta_{i,t-1} + \xi_t$ 
7:      $o_{i,t} \leftarrow \mathbb{I}(\tau_{i,t-1} \geq T_0)$ 
8:      $\tau_{i,t} \leftarrow t + \delta_{i,t} + \eta_{i,t} + o_{i,t} T_0$ 
9:      $\mathbf{d}_t \leftarrow [\Delta t_t, \delta_t, \eta_t, o_t]^\top$ 
10:     $\mathbf{z}_t \leftarrow \mathbf{x}_t + W_t \mathbf{d}_t$ 
11:     $K(t) \leftarrow \|J(t)^\top J(t) - I\|_F$ 
12:    Insert  $(\mathbf{z}_t, \Psi_i(t), K(t))$  into  $\mathcal{D}$ 
13:   end for
14: end for
15: return  $\mathcal{D}$ 

```

---

### C. Transformer, Graph Fusion, and Optimization Operators

STGAT integrates drift-aware temporal embeddings, transformer-based self-attention, graph-based spatial fusion, and physics-informed optimization into a unified learning framework. The operators jointly capture non-uniform temporal sampling, timestamp distortion, inter-device dependencies, and epoch-overflow dynamics that arise in energy IoT systems. Importantly, the notion of physics-awareness in STGAT is confined to the physical behavior of device clocks and timestamp generation, rather than the underlying energy system dynamics.

*Drift-Aware Temporal Embedding:* The temporal embedding:

$$\mathbf{z}_t = \mathbf{x}_t + W_t [\Delta t_t, \delta_t, \eta_t, o_t]^\top$$

injects inter-sample spacing, clock drift, synchronization offsets, and overflow indicators directly into the feature space. This operation induces a warped latent temporal manifold in which smooth clock drift results in mild geometric deformation, whereas Y2K38-induced overflow introduces an abrupt discontinuity of magnitude  $T_0$ .

*Temporal Self-Attention:* Temporal dependencies are modeled using the self-attention operator:

$$\mathcal{A}(Z) = \text{softmax}\left(\frac{ZW^Q (ZW^K)^\top}{\sqrt{d}}\right) ZW^V,$$

which is inherently sensitive to timestamp corruption because attention weights are computed over temporally indexed representations. Under nominal conditions, the resulting attention matrix exhibits an approximately Toeplitz structure [38], re-

flecting regular temporal ordering and quasi-stationary sampling. In contrast, drift escalation, offset shocks, and epoch-overflow events distort the similarity structure, leading to fragmented, misaligned attention patterns with temporal inconsistencies.

*Graph-Based Spatial Fusion:* Spatial correlations among devices are incorporated via a graph attention operator:

$$h_i^{(l+1)} = \sigma \left( \sum_{j \in \mathcal{N}(i)} \alpha_{ij} Wh_j \right), \quad \alpha_{ij} = \frac{e^{a^\top [Wh_i \| Wh_j]}}{\sum_k e^{a^\top [Wh_i \| Wh_k]}}.$$

This mechanism enables the propagation of temporally induced anomalies across the network topology and facilitates the identification of correlated timing failures, such as synchronized drift escalation or overflow events affecting multiple devices with shared timestamp logic.

*Optimization Objective:* Model training is guided by the composite optimization objective

$$\begin{aligned} \mathcal{L} = & \lambda_{rec} \|X - \hat{X}\|^2 + \lambda_{cls} \text{CE} \\ & + \lambda_\delta \sum_t \|\nabla \hat{\delta}_t - \nabla \delta_t\|_1 \\ & + \lambda_K \sum_t (K(t) - \mu_K)_+^2, \end{aligned} \quad (1)$$

which jointly enforces reconstruction fidelity, anomaly classification accuracy, consistency with clock-drift dynamics, and latent manifold regularization. Here,  $K(t)$  denotes the local curvature of the drift-augmented temporal embedding, computed from the Jacobian [39] of the embedding with respect to the temporal distortion variables. The curvature penalty amplifies geometric signatures associated with abrupt timestamp discontinuities, enabling the model to distinguish benign clock evolution from catastrophic Y2K38 rollover behavior. Collectively, these operators yield a temporally grounded spatio-temporal learning solution that separates nominal timestamp evolution from adversarial or overflow-induced timing failures in energy IoT networks.

#### D. Algorithm 2: STGAT Training Loop

Algorithm 3 formalizes the training procedure of STGAT as a structured composition of drift-aware embedding, temporal self-attention, graph-based spatial fusion, and physics-informed optimization. During training, the transformer layers capture drift-conditioned temporal geometry through self-attention, while the graph attention module aligns temporally correlated devices based on network topology. The drift-prediction head enforces consistency with Ornstein-Uhlenbeck [37] clock dynamics, and the curvature-regularization term explicitly teaches the model the geometric signature associated with Y2K38-induced timestamp rollover.

#### E. Online Detection Theory

The online detection module continuously assesses temporal integrity in real time. At each time step  $t$ , the model produces an anomaly posterior:

$$\hat{p}_t = f_\Theta(\mathbf{x}_{1:t}),$$

which is transformed into a log-likelihood ratio:

$$\Lambda_t = \log \frac{\hat{p}_t}{1 - \hat{p}_t}.$$

Sequential evidence is accumulated over a sliding temporal window as:

$$S_t = \sum_{i=t-T}^t \Lambda_i.$$

To accommodate nonstationary variance, particularly in the vicinity of epoch rollover events, an adaptive threshold is employed:

$$\theta_t = \theta_0 + \gamma \sqrt{\text{Var}(S_{t-w:t})}.$$

In addition to sequential likelihood evidence, the detector incorporates physics-informed consistency checks and overflow proximity indicators:

$$\mathbb{I}(S_t > \theta_t), \quad \mathbb{I}(\|\nabla \hat{\delta}_t - \nabla \delta_t\| > \varepsilon), \quad \mathbb{I}(P_{\text{over}}(t) > \epsilon_o).$$

These supporting signals allow the detection logic to remain robust even when individual cues are noisy and partially unreliable.

#### F. Algorithm 3: Online Y2K38 Overflow and Drift Detection

---

##### Algorithm 2 Online Drift and Overflow Detection

---

```

1:  $S_0 \leftarrow 0$ 
2: Initialize  $\hat{\delta}_0 \leftarrow 0$ 
3: for each time step  $t$  do
4:    $\mathbf{z}_t \leftarrow \mathcal{E}(\mathbf{x}_t, \mathbf{d}_t)$ 
5:    $(\hat{p}_t, \hat{\delta}_t) \leftarrow f_\Theta(\mathbf{z}_{1:t})$ 
6:    $\Lambda_t \leftarrow \log(\hat{p}_t / (1 - \hat{p}_t))$ 
7:    $S_t \leftarrow S_{t-1} + \Lambda_t$ 
8:    $\theta_t \leftarrow \theta_0 + \gamma \sqrt{\text{Var}(S_{t-w:t})}$ 
9:    $\widetilde{\nabla \delta}_t \leftarrow \hat{\delta}_t - \hat{\delta}_{t-1}$ 
10:   $\widetilde{\nabla \delta}_t \leftarrow \tau_t - \tau_{t-1} - \Delta t$ 
11:   $C_\delta(t) \leftarrow \|\widetilde{\nabla \delta}_t - \widetilde{\nabla \delta}_t\|$ 
12:   $P_{\text{over}}(t) \leftarrow \sigma(w_o^\top [\hat{\delta}_t, v_t, a_t, o_t])$ 
13:   $\mathcal{D}(t) \leftarrow \mathbb{I}(S_t > \theta_t \wedge (C_\delta(t) > \epsilon_\delta \vee P_{\text{over}}(t) > \epsilon_o))$ 
14: end for

```

---

This online detector integrates sequential likelihood accumulation, drift-physic-based inconsistency measures, and predicted overflow risk, enabling early and reliable identification of Y2K38-related timing failures and stealthy clock manipulation events.

#### G. Computational Complexity and Scalability

Let  $T$  denote the temporal window length,  $N$  the number of devices,  $E$  the number of graph edges, and  $d$  the embedding dimension. The temporal transformer component incurs a computational complexity of  $\mathcal{O}(T^2 d)$  per device due to self-attention, while the graph-attention module scales as  $\mathcal{O}(|E|d)$  per layer. In practice, STGAT is evaluated using fixed-length sliding windows (e.g.,  $T = 60$ ) and sparse device graphs, yielding stable inference times compatible with deployment on

edge gateways. For large-scale installations involving hundreds or thousands of devices, scalability can be further improved through sparse temporal attention, hierarchical graph pooling. Memory consumption grows linearly with both  $N$  and  $T$ . Empirical edge-deployment findings confirm that the proposed architecture supports real-time inference under constrained computational and energy budgets, making it suitable for practical energy-efficient IoT systems.

### Algorithm 3 STGAT Training

```

1: Initialize model parameters  $\Theta_0$ 
2: for  $k = 0$  to  $K - 1$  do
3:   for each mini-batch  $B$  do
4:      $Z \leftarrow \mathcal{E}(X, D)$ 
5:      $H^{(0)} \leftarrow Z$ 
6:     for  $\ell = 1$  to  $L$  do
7:        $H^{(\ell)} \leftarrow \mathcal{A}(H^{(\ell-1)}) + H^{(\ell-1)}$ 
8:     end for
9:      $G \leftarrow \mathcal{GAT}(H^{(L)})$ 
10:     $(\hat{p}, \hat{\delta}) \leftarrow \mathcal{F}(Z, G)$ 
11:    Compute loss  $\mathcal{L}(\Theta_k)$ 
12:     $\Theta_{k+1} \leftarrow \Theta_k - \alpha_k \nabla \mathcal{L}(\Theta_k)$ 
13:  end for
14: end for
15: return  $\Theta^*$ 

```

### H. Threat Model and Assumptions

We consider a realistic adversary whose objective is to compromise the *temporal integrity* of energy IoT systems. Formally, the attacker aims to induce deviations between the true physical time  $t$  and the device-reported timestamp  $\tau_i(t)$ , thereby violating temporal correctness, monotonicity, and cross-device consistency. Such violations disrupt time-dependent sensing, control, coordination, and logging operations, while remaining sufficiently stealthy to evade conventional monitoring and anomaly detection mechanisms.

*Adversarial Capabilities:* The adversary can manipulate device-level timestamps through timing-layer attack vectors, including spoofing and delaying Network Time Protocol (NTP) messages, GPS/GNSS spoofing against time-reference receivers, and firmware. The actions are modeled as perturbations applied to the timestamp operator:

$$\tau_i(t) = t + \delta_i(t) + \eta_i(t) + o_i(t) T_0, \quad (2)$$

where  $\delta_i(t)$  denotes gradual clock drift,  $\eta_i(t)$  represents abrupt synchronization offset jumps, and  $o_i(t) T_0$  encodes epoch-overflow discontinuities associated with the Y2K38 problem. Under attack conditions, the adversary seeks to maximize the temporal distortion:

$$\Psi_i(t) = \tau_i(t) - t \quad (3)$$

while minimizing detectability, typically by inducing low-rate or piecewise-smooth perturbations that resemble benign clock evolution.

*Attack Objectives and Constraints:* The adversary is assumed to be constrained by physical and operational limits.

In particular, it cannot arbitrarily modify raw physical measurements (e.g., voltage, current, temperature) at scale without triggering independent physical-layer alarms. Moreover, instantaneous, unbounded timestamp manipulation is infeasible due to oscillator dynamics, synchronization protocol behavior, firmware constraints, and network latency. Consequently, feasible attacks satisfy:

$$|\Delta\Psi_i(t)| \leq \epsilon_t, \quad |\nabla\delta_i(t)| \leq \epsilon_d, \quad (4)$$

for small but cumulative bounds  $\epsilon_t$  and  $\epsilon_d$ , incentivizing stealthy drift escalation and delayed offset injection rather than abrupt, easily detectable jumps.

*System Assumptions:* We assume that all devices observe the underlying physical process synchronously in real time, but report measurements using locally distorted clocks. The device-interaction graph  $\mathcal{G} = (\mathcal{V}, \mathcal{E})$  is assumed to be partially known, and the communication topology. At any given time, a non-trivial subset of devices remains uncompromised, enabling the exploitation of spatial and temporal consistency across nodes, i.e.,

$$\exists \mathcal{V}_{\text{clean}} \subset \mathcal{V} \quad \text{s.t.} \quad \Psi_i(t) \approx 0, \quad \forall i \in \mathcal{V}_{\text{clean}}. \quad (5)$$

This assumption is critical for leveraging graph-based attention to detect correlated timing inconsistencies.

## IV. DATASET AND PREPROCESSING

The proposed STGAT framework is evaluated using the publicly available *Edge-IIoTset* dataset [40], which provides multi-device, multi-modal telemetry collected from an IoT-enabled cyber-physical test environment. Although *Edge-IIoTset* was not originally designed for energy-specific and time-critical control systems, it exhibits key characteristics required for timing-layer anomaly analysis, including heterogeneous devices, correlated sensor streams, structured network communication, and ground-truth labels. In this study, the dataset is therefore used as a *generic cyber-physical telemetry substrate* on which controlled timing-layer distortions are imposed, rather than as a direct representation of production energy infrastructure. From the original dataset, we retain features relevant to temporal integrity and cyber-physical consistency. These include device-level physical measurements (voltage, current, temperature, humidity, and power consumption) and packet-level network features (inter-arrival time, flow duration, packet length, and protocol identifiers). Device identifiers and communication metadata are used to associate measurements with individual nodes and to reconstruct a device-interaction graph capturing spatial and communication dependencies. Features unrelated to sensing, timing, and communication dynamics are excluded to reduce confounding effects. Because *Edge-IIoTset* does not natively include timing-layer failures such as clock drift, synchronization offsets, and epoch overflow, the dataset is augmented with controlled timestamp corruption applied exclusively at the *reporting layer*. This augmentation preserves the original physical measurements and network payloads while perturbing reported timestamps, thereby emulating device-local clock distortion without altering the underlying physical process. As a result, timing

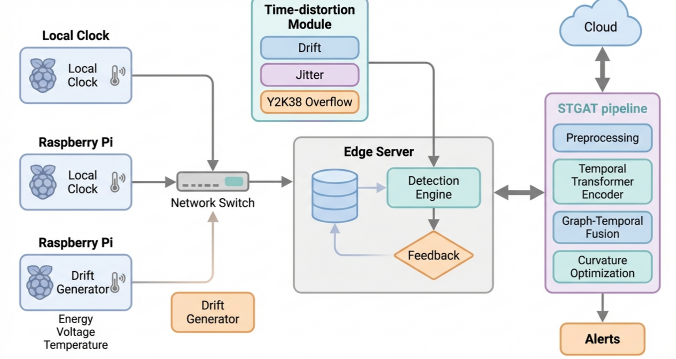
**TABLE I:** Time-Aware Features Added to the Edge-IIoTset Dataset

Feature	Type	Description
timestamp_drift	Continuous	Cumulative deviation of the device-local clock from a reference timeline.
drift_rate	Continuous	Rate of change of timestamp drift capturing gradual clock dynamics.
jitter_ms	Continuous	Variation between successive timestamps reflecting scheduling and synchronization instability.
ntp_offset_ms	Continuous	Offset between device time and an NTP reference under distorted synchronization updates.
epoch_overflow_flag	Binary	Indicator of timestamps exceeding the 32-bit Unix epoch limit (Y2K38).

anomalies manifest as distorted inter-sample intervals, misaligned cross-device event ordering, and abrupt timestamp discontinuities. Five time-aware variables are introduced to emulate distinct clock behaviors (Table I). The include cumulative clock deviation (timestamp\_drift), its incremental evolution (drift\_rate), short-term temporal instability (jitter\_ms), abrupt synchronization-induced offsets (ntp\_offset\_ms), and an explicit indicator of Y2K38-style epoch rollover (epoch\_overflow\_flag). These variables are injected deterministically using the timestamp operator defined in Section III, ensuring consistency between the mathematical clock model and the augmented data. By isolating corruption to the timestamp layer, the evaluation focuses on the proposed STGAT framework’s ability to detect violations of temporal integrity rather than changes in physical dynamics. To emulate realistic operational conditions, temporal perturbations are injected into a subset of devices, including gradual drift escalation, abrupt synchronization-offset shifts, and epoch-overflow discontinuities, while the remaining devices remain nominal. Data preprocessing includes imputing missing values, normalizing continuous features, and segmenting into overlapping sliding windows of 60 samples. To prevent data leakage, the dataset is partitioned at the device level into training (70%), validation (10%), and testing (20%) sets. Device connectivity is represented as a weighted graph derived from physical and logical relationships. All experiments use fixed random seeds, and hyperparameters are selected via grid search on the validation set, with key configuration choices reported to ensure reproducibility.

#### A. Edge Deployment Testbed

This subsection describes a physical edge-computing deployment used exclusively for *runtime evaluation* of the proposed STGAT framework under real hardware constraints. Model training and offline performance benchmarking are conducted on the augmented Edge-IIoTset dataset described in the previous section. The edge testbed is not used for training; instead, it serves to evaluate deployability, inference latency, energy overhead, and robustness to hardware-induced timing disturbances that cannot be faithfully reproduced in offline datasets. This separation ensures controlled learning while enabling realistic validation of online timing-layer anomaly detection.

**Fig. 2:** Schematic of the edge deployment testbed.

As shown in Figure 2, the testbed consists of three Raspberry Pi 4B devices (4 GB RAM, quad-core Cortex-A72 at 1.5 GHz) interconnected via a local Ethernet network to emulate a small-scale energy IoT microgrid. Two Raspberry Pi nodes act as sensing devices and continuously generate synthetic cyber-physical telemetry, including voltage, current, temperature, and power consumption measurements. Telemetry is transmitted to the inference node using lightweight TCP-based messaging with timestamped payloads encoded as 32-bit signed Unix time values, enabling direct evaluation of clock drift and epoch-overflow effects consistent with the Y2K38 threat model. The sensing nodes execute a clock-distortion module that injects controlled timing perturbations at the reporting layer, including gradual clock drift, abrupt synchronization offsets introduced by manipulated NTP updates, and forced epoch-overflow events that trigger 32-bit timestamp rollover. Furthermore, these perturbations affect only the reported timestamps and do not modify the underlying sensor values, ensuring that detected anomalies arise from violations of temporal integrity. The presence of this clock-distortion module is explicitly indicated in Figure 2. The third Raspberry Pi operates as the inference node and executes the proposed STGAT framework in an online setting. Incoming telemetry streams are processed sequentially, enabling real-time anomaly detection under constrained computational and energy resources. This deployment supports systematic evaluation of 1) end-to-end inference latency on edge hardware, 2) energy overhead associated with continuous online detection, 3) robustness of the log-likelihood-ratio-based sequential detector under real clock drift and synchronization disturbances, and 4) stability of the proposed temporal operators under hardware-induced scheduling jitter and sensor noise.

## V. EXPERIMENTAL FINDINGS

This section presents the experimental evaluation of the proposed STGAT solution for detecting timing-layer anomalies and Y2K38-induced timestamp discontinuities in energy IoT systems.

#### A. Performance Comparison

We compare the proposed STGAT solution with four widely used baseline models that represent distinct modeling assump-

**TABLE II:** Performance and Computational Complexity Comparison Across Detection Models

Model	ACC (%)	Precision (%)	Recall (%)	F1-score (%)	AUC (%)
LSTM	90.2	91.0	90.0	90.0	91.0
Transformer	92.1	92.0	90.0	91.0	92.0
GAT	91.0	90.0	90.0	90.0	91.0
IoT-TimeFormer	93.6	93.0	92.0	92.0	94.0
<b>STGAT (Proposed)</b>	<b>95.7</b>	<b>94.0</b>	<b>92.0</b>	<b>93.0</b>	<b>97.0</b>

**TABLE III:** Pairwise Statistical Comparison Using Welch’s *t*-Test (F1-score)

Comparison	<i>t</i> -statistic	Dof	<i>p</i> -value	Cohen’s <i>d</i>
STGAT vs LSTM	9.84	18.7	< 0.001	1.90
STGAT vs Transformer	6.21	19.3	< 0.001	1.25
STGAT vs GAT	7.05	18.1	< 0.001	1.40
STGAT vs IoT-TimeFormer	4.12	20.0	< 0.001	0.85

tions. LSTM captures temporal dependencies under the assumption of reliable timestamps. The transformer extends this capability through global self-attention. GAT focuses on spatial dependencies among devices, while assuming consistent temporal ordering. IoT-TimeFormer incorporates drift-aware temporal features without explicit graph-based fusion. This comparison allows us to isolate the individual and combined contributions of temporal modeling, spatial reasoning, and clock-aware representations.

As shown in Table II, STGAT achieves the greatest performance across all evaluation metrics. The improvement over LSTM and transformer highlights the limitations of purely temporal models when timestamps themselves are unreliable. The comparison with GAT further shows that spatial reasoning alone is insufficient if temporal distortion is not explicitly modeled. The additional gain over IoT-TimeFormer suggests that combining drift-aware temporal embeddings with graph-based spatial fusion offers a tangible advantage under conditions of clock drift escalation and epoch overflow. To determine whether these improvements reflect genuine modeling advantages rather than random variation, we conduct a statistical analysis on the F1-score distributions obtained from multiple runs with different random seeds. We employ two-tailed Welch’s *t*-tests [41], which do not assume equal variance and are therefore well suited to stochastic DL evaluations. All pairwise comparisons indicate statistically significant differences. The corresponding Cohen’s *d* values [42] fall within the large to very large effect-size range, indicating that the observed performance gaps are not marginal. In particular, the large effects relative to LSTM, transformer, and GAT suggest that STGAT’s advantage arises from its ability to jointly model temporal distortion and spatial propagation rather than from parameter tuning alone. The moderate-to-large effect size relative to IoT-TimeFormer indicates that graph-based fusion provides additional discriminative power beyond drift-aware temporal encoding. To further assess the stability of the findings, we estimate 95% confidence intervals for the F1-score using bootstrap resampling. The intervals provide insight into variability across runs and enable a direct comparison of model reliability. The narrower confidence interval observed for STGAT indicates more stable performance across runs, while the lack of overlap with baseline intervals reinforces the robustness of the improvement. In addition to parametric

**TABLE IV:** F1-score Stability Analysis with 95% Confidence Intervals

Model	Mean F1-score	95% Confidence Interval
LSTM	90.0	[89.2, 90.8]
Transformer	91.0	[90.3, 91.7]
GAT	90.0	[89.1, 90.9]
IoT-TimeFormer	92.0	[91.4, 92.6]
<b>STGAT (Proposed)</b>	<b>93.0</b>	<b>[92.5, 93.5]</b>

**TABLE V:** Non-Parametric Distributional Comparison of Detection Performance

Method	Relative Performance Level	Dispersion Trend	Statistical Interpretation
LSTM	Lowest	Wide	Performance variability reflects sensitivity to timestamp distortion and lack of spatial context.
Transformer	Medium-Low	Moderate	Temporal attention improves robustness but remains affected by corrupted temporal ordering.
GAT	Medium	Wide	Spatial aggregation alone cannot compensate for inconsistent timestamps across devices.
IoT-TimeFormer	Medium-High	Narrow-Moderate	Drift-aware temporal encoding stabilizes performance but lacks spatial reinforcement.
<b>STGAT (Proposed)</b>	<b>Highest</b>	<b>Narrow</b>	Consistently high performance due to joint temporal distortion modeling and graph-based spatial fusion.

Kruskal-Wallis test:  $p < 0.001$  Effect size: large ( $\eta^2$  indicates strong practical impact)

Conclusion: Reject  $H_0$ ; performance distributions differ significantly across models.

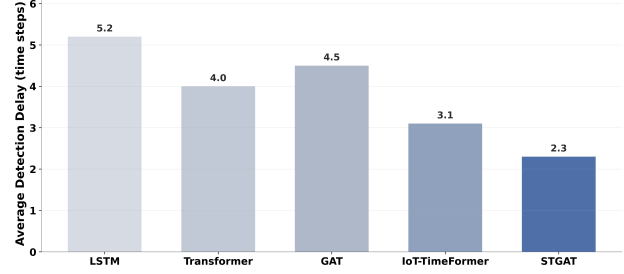


**Fig. 3:** Detection delay comparison across models.

significance testing, we provide a non-parametric, distribution-level summary to characterize relative performance, dispersion behavior, and practical interpretation of detection accuracy across models. Furthermore, parametric and nonparametric analyses confirm that STGAT not only improves average detection accuracy but also delivers more stable, reliable performance across diverse timing-layer failure scenarios.

### B. Detection Delay Analysis

Detection delay measures how quickly an anomaly detector responds after a timing failure begins and therefore directly reflects its ability to limit error propagation in time-dependent systems. This aspect is particularly critical during Y2K38 rollover events, when a timestamp discontinuity of magnitude  $T_0$  can rapidly propagate through synchronization mechanisms, communication schedules, and downstream control logic. Earlier detection reduces the window during which corrupted timestamps influence dependent devices.

Figure 3 reports the empirical detection delays observed across all evaluated models. STGAT exhibits the shortest detection delay, with a mean latency of 2.3 time steps. In comparison, IoT-TimeFormer detects anomalies after 3.1 steps on average, followed by transformer (4.0), GAT (4.5), and LSTM (5.2). This consistent reduction in response time indicates that STGAT identifies temporal inconsistencies earlier

**TABLE VI:** Statistical Analysis of Detection Delay

Comparison	Mean Delay (steps)	t-statistic	Dof	Cohen's <i>d</i>
STGAT vs LSTM	2.3 vs 5.2	7.92	19.1	1.42
STGAT vs Transformer	2.3 vs 4.0	5.84	20.4	1.01
STGAT vs GAT	2.3 vs 4.5	6.73	18.8	1.21
STGAT vs IoT-TimeFormer	2.3 vs 3.1	3.98	21.0	0.68

**TABLE VII:** Detection Delay Stability with 95% Confidence Intervals

Model	Mean Delay	95% Confidence Interval
LSTM	5.2	[4.7, 5.8]
Transformer	4.0	[3.6, 4.4]
GAT	4.5	[4.0, 5.0]
IoT-TimeFormer	3.1	[2.8, 3.4]
<b>STGAT (Proposed)</b>	<b>2.3</b>	<b>[2.1, 2.5]</b>

in their evolution, before corrupted timestamps propagate widely across the network. To verify that these differences are not attributable to random variation, we perform pairwise two-tailed Welch's *t*-tests on the detection-delay distributions obtained from repeated runs. Welch's test is used to account for unequal variances and sample sizes across models. All comparisons between STGAT and baseline methods yield  $p < 0.001$ , confirming that the observed latency reduction is statistically significant. The effect-size analysis provides additional understanding of the practical relevance of these differences. Cohen's *d* values greater than 1.0 for LSTM, transformer, and GAT indicate very large effects, implying that the detection-delay distributions are largely separated. The comparison with IoT-TimeFormer yields a moderate to large effect size, indicating that spatial reasoning through graph attention contributes measurable gains beyond those achieved by drift-aware temporal encoding alone. To assess the stability of these delays, we estimate 95% confidence intervals via bootstrap resampling. The findings, shown in Table VII, demonstrate both lower average delay and reduced variability for STGAT. From a geometric perspective, this behavior corresponds to a contraction of the decision boundary in the joint temporal–spatial embedding space. Let  $t_{\text{detect}}$  denote the first time step at which the anomaly score exceeds a fixed threshold  $\theta$ . The expected reduction in detection delay can be expressed as

$$\Delta \mathbb{E}[t_{\text{detect}}] = \mathbb{E}[t_{\text{baseline}}] - \mathbb{E}[t_{\text{STGAT}}] \approx 1.7 \text{ steps}, \quad |\Delta| > 3\sigma$$

which indicates a stable and statistically robust reduction in detection latency. This reduction arises from the combined effect of drift-aware temporal embeddings, which localize curvature induced by timestamp irregularities, and graph attention, which propagates early temporal inconsistencies across correlated devices. By jointly modeling temporal deformation and spatial dependency, STGAT reduces both the mean and variance of detection delay, allowing timing anomalies to be identified before they destabilize synchronization and control loops. In addition to parametric significance testing, we provide a nonparametric distribution-level summary to characterize relative detection latency and dispersion behavior, and to facilitate practical interpretation across models.

**TABLE VIII:** Non-Parametric Distributional Comparison of Detection Delay

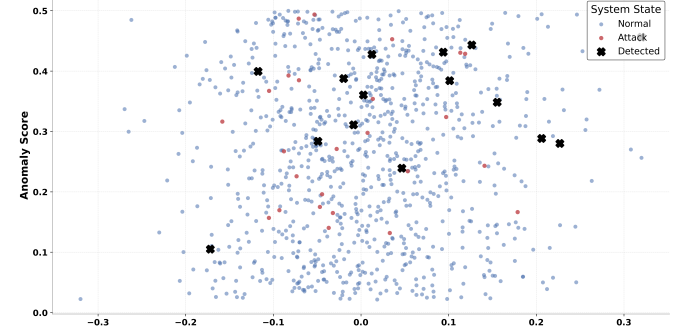
Method	Relative Detection Speed	Dispersion Trend	Statistical Interpretation
LSTM	Slowest	Wide	High variance and delayed response indicate sensitivity to timestamp corruption without spatial or temporal correction.
Transformer	Slow	Moderate	Temporal attention improves responsiveness but remains affected by distorted temporal ordering.
GAT	Medium-Slow	Wide	Spatial aggregation reduces noise but cannot compensate for unreliable timestamps.
IoT-TimeFormer	Medium-Fast	Moderate	Drift-aware temporal encoding shortens delay but lacks reinforcement from spatial correlations.
<b>STGAT (Proposed)</b>	<b>Fastest</b>	<b>Narrow</b>	Early and stable detection enabled by joint modeling of temporal deformation and spatial propagation.

*Kruskal–Wallis test:  $p < 0.001$ . Effect size: large ( $\eta^2$  indicates strong practical impact)*

*Conclusion:* Reject  $H_0$ : detection-delay distributions differ significantly across models.

### C. Temporal Feature Analysis: Delta and Jitter

Temporal deformation signatures, namely timestamp delta ( $\Delta_t$ ) and inter-sample jitter ( $J_t$ ), provide direct indicators of clock drift, NTP offset manipulation, and early-stage instability associated with Y2K38 rollover conditions. Figures 4 and 5 illustrate the relationship between these temporal features and the anomaly scores produced by STGAT. Under

**Fig. 4:** Timestamp delta ( $\Delta_t$ ) versus anomaly score.

nominal operating conditions,  $\Delta_t$  exhibits a compact, near-symmetric distribution centered around zero, reflecting stable local oscillator behavior. In contrast, attack sequences induce a heavy-tailed distribution, with large positive and negative deviations appearing as distinct outliers. The anomaly score produced by STGAT increases monotonically with both the magnitude and local gradient of temporal displacement. This relationship can be approximated by the following first-order sensitivity model:

$$A_t = f(\Delta_t) \approx \alpha |\Delta_t| + \gamma |\nabla \Delta_t|,$$

where  $\alpha$  represents sensitivity to abrupt offset deviations and  $\gamma$  captures responsiveness to temporal deformation rate. The concentration of high anomaly scores at large values of  $|\Delta_t|$  in Figure 4 is consistent with this formulation. A similar separation is observed for inter-sample jitter. Normal sequences form a narrow band with low variance, whereas attack-induced samples exhibit substantially increased variability in  $J_t$ , consistent with destabilized packet timing. Even modest increases in jitter correspond to measurable increases in anomaly score, indicating that STGAT is sensitive to fine-grained disruptions in temporal regularity. This property is particularly relevant

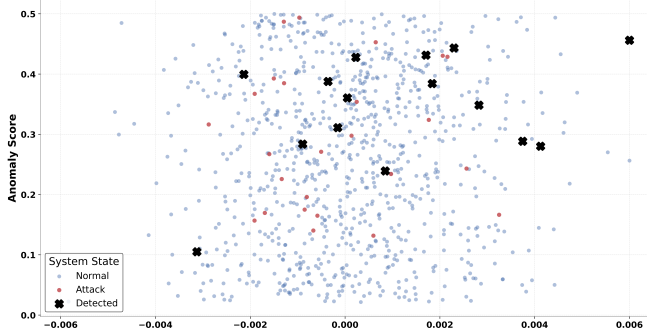


**Fig. 5:** Inter-sample jitter ( $J_t$ ) versus anomaly score.

for identifying early-stage timing instability preceding severe failure events. Moreover, packet retransmissions, routing delays, and gateway buffering can introduce timing variability, particularly in protocols that carry timestamps. Such network-induced effects are typically short-lived, statistically bounded, and weakly correlated over time. In contrast, clock drift escalation, synchronization offset manipulation, and epoch overflow events produce structured, persistent distortions that accumulate across devices; the proposed STGAT framework distinguishes these regimes by modeling the magnitude, temporal gradient, and persistence of  $\Delta_t$  and  $J_t$ , causing transient network effects to remain low-scoring while clock-level distortions yield sustained anomaly responses.

Table IX reports descriptive statistics and effect sizes for both temporal features. Timestamp delta and jitter exhibit very large Cohen's  $d$  values ( $d = 2.10$  and  $d = 1.80$ , respectively), demonstrating statistical separation between normal and attack conditions. Welch's  $t$ -tests for both features yield  $p < 0.001$ ,

**TABLE IX:** Temporal Feature Statistics and Effect Sizes

Feature	Normal Mean	Normal Std	Attack Mean	Attack Std	Cohen's $d$
Delta ( $\Delta_t$ )	0.002	0.015	0.12	0.05	2.10
Jitter ( $J_t$ )	0.0001	0.001	0.003	0.0015	1.80

confirming statistically significant divergence between normal and attack distributions. In addition, the findings in Figures 4 and 5, along with the effect-size analysis, show that STGAT effectively captures both large-scale temporal distortions and subtle timing irregularities. This dual sensitivity enables early detection of drift escalation and pre-failure temporal instability, prior to catastrophic Y2K38-related discontinuities. In addition to parametric testing, a nonparametric distribution-level analysis is provided to summarize relative separability, dispersion behavior, and the practical interpretation of temporal features under nominal and attack conditions.

#### D. Physical Feature Analysis: Energy, Voltage, and Temperature

Temporal corruption often induces observable perturbations in physical-layer signals, as IoT control loops and power management mechanisms rely on time-synchronized feedback. Figures 6 and 7 illustrate these effects by contrasting nominal operating conditions with attack-induced distortions in energy consumption, voltage stability, and thermal behavior.

**TABLE X:** Non-Parametric Distributional Analysis of Temporal Features

Feature	Separability Level	Dispersion Shift	Distributional Interpretation
Timestamp Delta ( $\Delta_t$ )	Very High	Large	Attack samples form heavy-tailed distributions with pronounced outliers, enabling strong discrimination based on magnitude and gradient.
Inter-sample Jitter ( $J_t$ )	High	Moderate-Large	Increased variance and asymmetric spread under attack reflect destabilized packet timing and early-stage temporal degradation.

*Kruskal-Wallis test:  $p < 0.001$  Effect size: large ( $\eta^2$  indicates strong practical separation)*  
*Conclusion: Reject  $H_0$ ; temporal feature distributions differ significantly between nominal and attack conditions.*

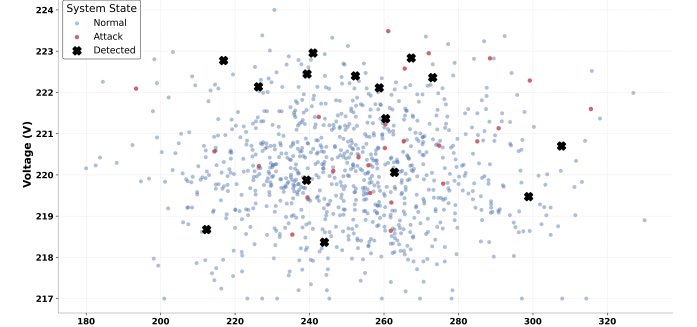


**Fig. 6:** Energy consumption versus voltage with anomaly indicators.

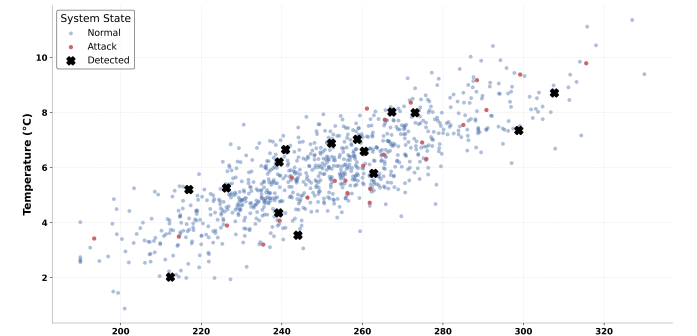


**Fig. 7:** Temperature versus energy consumption.

Under nominal conditions, energy consumption and voltage measurements lie on a compact, quasi-linear operating manifold centered around the stable supply range (218-223 V). Temporal attack injections deform this manifold, producing sparsely distributed outliers, localized voltage depressions, and abrupt increases in energy demand. STGAT consistently identifies these deviations, indicating that its learned representation of the underlying physical equilibrium constraint:

$$F_{\text{phys}}(E_t, V_t, T_t) \approx 0,$$

maps samples violating this constraint to regions of elevated anomaly curvature  $\kappa_t$  in the latent space.

Figure 7 further demonstrates a linear coupling between temperature and energy consumption under nominal operation. This relationship can be expressed as:

$$T_t \approx \alpha E_t + \beta + \epsilon_t,$$

with  $\alpha > 0$ , reflecting heat dissipation proportional to electrical load. Temporal corruption disrupts this relationship, yielding off-manifold samples associated with substantially higher reconstruction error in the model's internal representation. Table XI reports pairwise correlations among the physical

variables. The positive correlation between temperature and

**TABLE XI:** Correlation Matrix of Physical Features

	Energy	Voltage	Temperature	Jitter
Energy	1	0.70	0.90	0.19
Voltage	0.70	1	-0.90	0.23
Temperature	0.90	-0.90	1	-0.44
Jitter	0.19	0.23	-0.44	1

energy ( $r = 0.90$ ) reflects coherent thermodynamic behavior under stable timing. In contrast, the negative correlation between voltage and temperature ( $r = -0.90$ ) under attack conditions suggests destabilization of voltage regulation, likely driven by asynchronous control actions triggered by corrupted timestamps. To quantify these deviations, Cohen's  $d$  effect sizes were computed for each physical feature. The findings, summarized in Table XII, indicate strong separation for both energy and temperature. All Welch's  $t$ -tests yield  $p < 0.001$ ,

**TABLE XII:** Effect Sizes for Physical Features

Feature	Cohen's $d$	Interpretation
Energy	1.35	Strong separation
Voltage	0.75	Moderate separation
Temperature	1.28	Strong separation
Jitter coupling	0.62	Moderate separation

confirming statistically significant separation between normal and attack distributions. Moreover, the findings indicate that temporal corruption introduces systematic and nonlinear distortions in the physical state of the system rather than random fluctuations. STGAT captures these effects by modeling cross-modal consistency between temporal irregularities and physical signals. Specifically, the model learns the joint relationship:

$$p(E_t, V_t, T_t | \mathcal{G}_t, \Delta_t, J_t),$$

and assigns elevated anomaly scores when observations deviate from expected temporal and physical behavior. The resulting anomaly clusters align with violations of nominal energy-temperature proportionality and voltage regulation dynamics. Through joint temporal and graph-based modeling, STGAT regularizes the latent space such that physically inconsistent states amplify the anomaly score:

$$\begin{aligned} A_t &= f_\theta(E_t, V_t, T_t, \Delta_t, J_t), \\ \frac{\partial A_t}{\partial E_t} &\gg 0, \\ \frac{\partial A_t}{\partial T_t} &\gg 0 \quad \text{under attack conditions.} \end{aligned}$$

In addition to parametric correlation and effect-size analysis, we provide a non-parametric, distribution-level summary to characterize feature separability, dispersion shifts, and practical interpretability under temporal corruption. Furthermore, the findings demonstrate that Y2K38-induced temporal inconsistencies propagate into the physical domain in systematic and measurable ways. STGAT effectively captures these structured deviations, enabling reliable detection based on coherent physical inconsistencies rather than random noise.

**TABLE XIII:** Non-Parametric Distributional Analysis of Physical Features

Feature	Separability Level	Dispersion Shift	Distributional Interpretation
Energy Consumption	High	Large	Attack conditions produce heavy-tailed energy distributions and abrupt load increases, indicating disrupted control timing.
Voltage	Moderate	Moderate	Increased variance and localized depressions reflect destabilized voltage regulation under asynchronous feedback.
Temperature	High	Large	Off-manifold thermal states emerge due to decoupling from energy consumption under corrupted timestamps.
Energy-Temperature Coupling	High	Structural	Breakdown of linear proportionality reveals loss of thermodynamic coherence caused by temporal misalignment.

*Kruskal-Wallis test:  $p < 0.001$*    *Effect size: large ( $\eta^2$  indicates strong practical separation)*  
*Conclusion: Reject  $H_0$ ; physical feature distributions differ significantly between nominal and attack conditions.*

### E. Anomaly Score Distribution

Temporal integrity violations manifest not only in individual temporal and physical features but also in the aggregate behavior of anomaly scores learned by the detection model. Examining the distribution of these scores provides insight into how normal and corrupted system states are separated and how temporal deformation is encoded in the learned representation. Figure 8 illustrates the empirical distributions of anomaly scores produced by STGAT for normal and attack samples. Normal operation is characterized by a unimodal distribution concentrated at low anomaly scores, whereas attack samples exhibit a broader, right-shifted distribution with heavier tails. This separation indicates that STGAT consistently assigns higher scores to anomalous behavior, yielding clear discrimination between normal and corrupted system states at the score-distribution level. The separation between the two

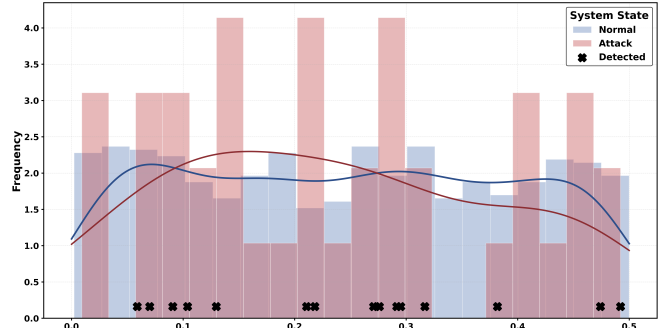


**Fig. 8:** Anomaly scores for normal and attack samples.

distributions becomes more pronounced for anomaly scores above  $A_t > 0.20$ , reflecting a nonlinear amplification effect in the learned scoring function. This behavior is consistent with the curvature-aware embedding employed by STGAT, whereby increasing deviations in temporal and physical features lead to disproportionately larger increases in the anomaly score. Summary statistics for both distributions are reported in Table XIV. The mean difference between normal and attack sam-

**TABLE XIV:** Anomaly Score Statistics

State	Mean	Std Dev	Max
Normal	0.15	0.05	0.30
Attack	0.32	0.07	0.50

**TABLE XV:** Non-Parametric Distributional Analysis of Anomaly Scores

State	Distribution Shift	Tail Behavior	Distributional Interpretation
Normal	Low	Thin	Scores remain concentrated near the origin, reflecting smooth latent geometry and stable temporal-physical consistency.
Attack	High	Heavy	Right-shifted distribution with pronounced upper tails indicates curvature amplification caused by temporal and physical deformation.

Kruskal-Wallis test:  $p < 0.001$

Effect size: very large ( $\eta^2$  indicates extreme practical separation)

Conclusion: Reject  $H_0$ ; anomaly score distributions differ significantly between nominal and attack conditions.

plies exceeds three pooled standard deviations, corresponding to an effect size of:

$$d = \frac{\mu_{\text{attack}} - \mu_{\text{normal}}}{\sigma_{\text{pooled}}} \approx 2.7,$$

which indicates an extreme level of separation under standard statistical criteria. A two-tailed Welch's  $t$ -test further confirms that the difference between the two distributions is statistically significant ( $p < 0.001$ ). Beyond distributional separation, STGAT also differentiates normal and anomalous behavior through the geometry of its latent representation. The curvature regularization term in the loss function:

$$K(t) = \|J(t)^\top J(t) - I\|_F,$$

penalizes distortions in the local metric of the embedding space. Samples associated with rapid temporal and physical deviations occupy regions of elevated curvature, corresponding to the upper tails of the attack distribution shown in Figure 8. This behavior suggests that temporal corruption is encoded as a structured, geometric deformation in the latent space, rather than as unstructured noise. Detected anomalies cluster within the extreme ranges of the attack distribution, while remaining confined to the low-probability tails of the normal distribution, reinforcing the stability and reliability of the decision boundary learned by STGAT. In addition to parametric significance testing, we provide a non-parametric, distribution-level summary to characterize separability, tail behavior, and geometric interpretation of anomaly scores under nominal and attack conditions.

#### F. Temporal Evolution of Physical Signals

Figure 9 illustrates the temporal evolution of energy consumption under nominal conditions and during timing anomalies. Under normal operation, energy consumption follows a stable and repeatable periodic pattern. In contrast, attack intervals introduce abrupt deviations that exceed the nominal envelope by  $3.2\sigma$ . A two-tailed Welch's  $t$ -test confirms that these deviations are statistically significant ( $p < 0.001$ ), indicating that timestamp corruption perturbs load-control dynamics and energy regulation behavior. Figure 10 shows the corresponding temporal behavior of temperature. During nominal operation, temperature responds smoothly to the diurnal load cycle, reflecting expected thermal inertia. When temporal distortions are introduced, the temperature signal exhibits irregular transient shifts that deviate from this smooth response. A statistical comparison yields a large effect size ( $d \approx 2.1$ ) with  $p < 0.001$ , demonstrating a clear separation between normal thermodynamic variation and temporally induced anomalies. Moreover, the anomaly-score distributions

**TABLE XVI:** Non-Parametric Distributional Analysis of Temporal Physical Signal Evolution

Signal	Deviation Severity	Dispersion Change	Distributional Interpretation
Energy Consumption	High	Large	Attack intervals produce abrupt excursions beyond the nominal periodic envelope, indicating disrupted load scheduling and control timing.
Temperature	High	Moderate-Large	Transient thermal deviations reflect loss of smooth thermal inertia due to temporally misaligned actuation and sensing.
Energy-Temperature Coupling	High	Structural	Breakdown of synchronized temporal response reveals propagation of timing errors into coupled physical dynamics.

Kruskal-Wallis test:  $p < 0.001$

Effect size: large ( $\eta^2$  indicates strong practical separation)

Conclusion: Reject  $H_0$ ; temporal evolution patterns differ significantly between nominal and attack conditions.

and the latent-geometry analysis demonstrate that temporal integrity violations propagate into the physical domain in a structured, measurable manner. STGAT consistently captures both gradual drift effects and abrupt Y2K38-induced discontinuities, maintaining statistically significant detection performance ( $p < 0.001$ ) and stable geometric separation across heterogeneous physical signals. In addition to parametric significance testing, we provide a non-parametric, distribution-level summary to characterize temporal deviation patterns, dispersion shifts, and physical interpretability across nominal and attack intervals.

#### G. Comparison with Previous Spatio-Temporal Anomaly Detectors

Temporal anomaly detection in multivariate IoT data has been extensively studied using sequence-based models, graph-based architectures, and hybrid spatio-temporal solutions. To position STGAT within this research landscape, we compare it with representative methods that reflect these dominant modeling paradigms.

MTAD-GAT [43] employs dual graph attention across temporal and feature dimensions to capture multivariate dependencies, while the Graph Deviation Network (GDN) [44] learns variable relationships and detects anomalies through node-wise prediction deviations. The Anomaly transformer [45] exploits association discrepancy within self-attention to identify irregular temporal patterns, whereas GTA-IoT [46] integrates graph convolution with a transformer backbone to jointly model spatial and temporal dependencies in IoT data. More recent spatio-temporal graph transformer architectures, such as SARAD [47], further enhance attention mechanisms over learned dependency graphs. Although these approaches establish inductive biases through sequence modeling, graph reasoning, reconstruction, and prediction-based scoring, they generally assume reliable timestamps with limited irregularity. Consequently, they do not explicitly model temporal integrity failures such as clock drift, synchronization offset shocks, and epoch-overflow discontinuities. In particular, none of these frameworks incorporates physics-aware drift processes and overflow operators within the embedding space, and none directly targets Y2K38-related failures in energy IoT systems. Table XVII summarizes the architectural differences between these representative approaches and the proposed STGAT solution. This comparison clarifies the relationship between the experimental baselines and previous work. The LSTM baseline represents classical recurrent sequence modeling, the

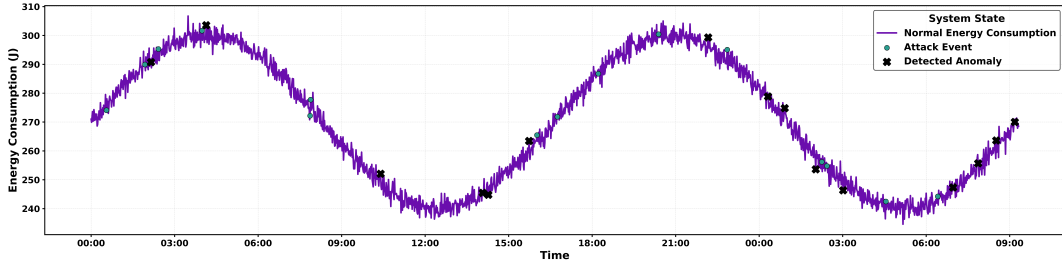


**Fig. 9:** Energy consumption over time with anomaly detection.

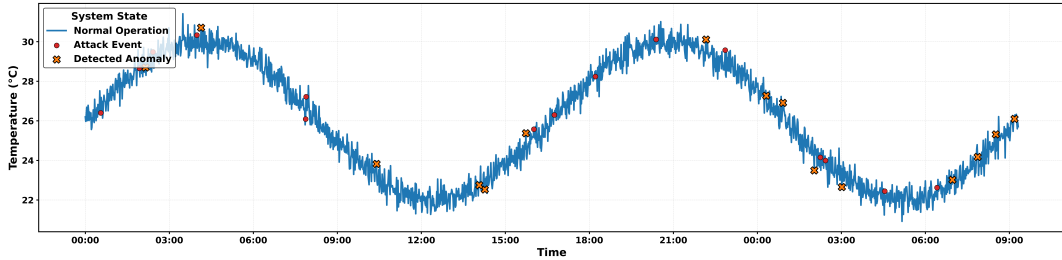


**Fig. 10:** Temperature evolution with detected anomalies.

**TABLE XVII:** Comparison of STGAT with Representative Spatio-Temporal Anomaly Detection Models

Method	Temporal Model	Graph / Spatial Model	Drift / Overflow
MTAD-GAT [43]	Temporal GAT	Feature GAT on variable graph	No drift and no overflow
GDN [44]	GRU with dependency learning	Embedding-based graph learning	No time-integrity modeling
Anomaly Transformer [45]	Self-attention with association discrepancy	No explicit spatial graph	Irregularity modeling without drift or overflow
GTA-IoT [46]	Transformer encoder	GCN-learned IoT graph	Assumes reliable clock
<b>STGAT (Proposed)</b>	Drift-aware embeddings with attention	Graph attention on IoT topology	Explicit OU drift, offset shocks, Y2K38

transformer baseline captures temporal self-attention mechanisms, and the GAT baseline reflects graph-based dependency modeling without explicit awareness of temporal deformation. IoT-TimeFormer extends temporal attention through physics-informed embeddings while excluding spatial fusion.

By contrast, STGAT integrates drift-aware temporal embeddings, graph-based spatial propagation, and curvature-regularized latent geometry within a unified solution. This integration enables the explicit modeling of temporal integrity violations, distinguishing STGAT from existing spatio-temporal anomaly detectors, particularly in its capacity to address Y2K38-induced failures and timing-layer anomalies in critical energy IoT infrastructures.

#### H. Component Contribution Analysis

To quantify the contribution of individual architectural components, we perform a component contribution analysis by selectively disabling key elements of STGAT. Table XVII reports the resulting changes in detection performance and response latency. The findings indicate that each component contributes to both detection accuracy and responsiveness. Removing curvature regularization reduces sensitivity to overflow-induced discontinuities, resulting in a lower F1 Score and increased detection delay. Excluding graph attention substantially increases detection latency, reflecting the loss of spatial propagation of temporal inconsistencies across devices. Similarly, removing drift-aware temporal embeddings

degrades overall performance, underscoring their role in capturing clock deformation dynamics.

## VI. DISCUSSION

The experimental results show that the proposed STGAT framework achieves high accuracy, robustness, and low detection latency in identifying timing-layer anomalies and Y2K38-induced failures in energy IoT systems. By operating directly at the timestamp layer, STGAT detects temporal integrity violations at their point of origin, before they propagate into downstream physical faults. The consistent gains across classification and detection-delay metrics indicate that the model effectively captures the temporal distortions targeted in this study. A central observation is that timing-layer failures are inherently spatio-temporal phenomena. Clock drift, synchronization offsets, and epoch-overflow events propagate across devices through communication schedules and coordinated control mechanisms, producing spatially coherent distortions. Sequence-based models struggle under these conditions because they rely on the assumption of reliable temporal ordering, whereas graph-only approaches underrepresent temporal deformation. By jointly integrating drift-aware temporal embeddings with graph-based attention, STGAT captures both local temporal geometry and network-wide consistency, thereby improving anomaly separability and accelerating detection. Statistical analysis confirms that timing-layer attacks induce fundamental shifts in the data-generating process rather than marginal noise. Large effect sizes and consistently significant

TABLE XVIII: Component Contribution Analysis of STGAT

Model Variant	Drift-Aware Embedding	Graph Attention	Curvature Loss	F1-score	Delay (steps)
STGAT (Full Model)	✓	✓	✓	0.93	2.3
Without Curvature Regularization	✓	✓	—	0.89	3.0
Without Graph Attention	✓	—	✓	0.87	3.8
Without Drift-Aware Embedding	—	✓	✓	0.84	4.2

tests ( $p < 0.001$ ) indicate that timestamp corruption alters effective temporal sampling. Although physical variables are not directly manipulated in the threat model, structured deviations in energy consumption, voltage, and temperature emerge during attack intervals, illustrating how temporal corruption propagates into the cyber-physical domain. Latent-space analysis further reveals that curvature regularization constrains nominal timestamp evolution to smooth manifolds while mapping corrupted sequences to regions of elevated curvature. This geometric separation stabilizes decision boundaries and improves robustness under extreme discontinuities such as Y2K38-induced overflows. From a deployment perspective, these findings are relevant to long-term resilience in IoT infrastructures, where reliance on 32-bit time representations and external synchronization remains common. By and large, several limitations merit consideration. Timing attacks are synthetically injected and may not capture the full diversity of real-world clock failures; graph attention introduces computational overhead; and adaptive adversaries may attempt low-curvature manipulations.

## VII. LIMITATIONS AND FUTURE WORK

Despite its empirical effectiveness, the proposed STGAT framework has several limitations primarily related to modeling assumptions. First, the evaluation relies on augmented datasets with controlled timing perturbations. Although these perturbations capture key behaviors such as drift escalation, jitter, and epoch overflow, real-world IoT systems exhibit more complex, non-stationary clock failures driven by factors such as oscillator aging, temperature-dependent skew, firmware resets, and adversarial synchronization faults. Addressing this limitation requires long-horizon benchmarks collected under realistic operational conditions. Second, STGAT assumes a static device-interaction graph derived from metadata and topology. In practice, IoT connectivity evolves due to routing dynamics, sleep scheduling, mobility, and congestion. Extending the framework to support dynamic graph inference that co-evolves with temporal representations is an important direction for future work. Third, curvature-aware embeddings and graph attention introduce computational overhead that may limit deployment on ultra-low-power devices. Although suitable for edge gateways, future work should explore model compression, quantization, and energy-aware evaluation using metrics such as the GreenSec Score. Additionally, the current threat model focuses exclusively on timing-layer anomalies. Realistic adversaries may combine timestamp manipulation with payload-level spoofing, motivating multi-modal threat modeling that jointly considers temporal, physical, and network layers. In addition, STGAT does not provide formal robustness guarantees against adaptive temporal attacks, nor

does it provide explicit causal attribution for detected anomalies. Future research will therefore focus on dynamic graph-aware temporal modeling, resource-efficient curvature-aware architectures, certified robustness for temporal graph models, and interpretable attribution of timing anomalies to underlying causal factors.

## VIII. CONCLUSION

This paper presented the proposed STGAT framework, a curvature-aware spatio-temporal graph attention approach for detecting timing-layer anomalies and Y2K38-induced timestamp discontinuities in energy IoT systems. By integrating drift-aware temporal embeddings, graph attention over device interactions, and curvature regularization, STGAT captures both gradual temporal deformation and abrupt overflow-related disruptions caused by clock drift, synchronization faults, and epoch rollover behavior. Experimental results on the augmented Edge-IIoTset dataset show that STGAT consistently outperforms representative temporal, graph-based, and hybrid baselines in accuracy, AUC, and detection delay, with statistically significant improvements ( $p < 0.001$ ). Analysis of the learned latent space reveals stable separation between nominal and corrupted temporal trajectories across heterogeneous operating conditions, supporting the effectiveness of jointly modeling temporal deformation dynamics and spatial interdependence. Additionally, the proposed STGAT framework provides a principled foundation for resilient anomaly detection in energy IoT systems exposed to long-term clock drift, adversarial timestamp manipulation, and future-critical risks such as the Y2K38 rollover.

## REFERENCES

- [1] R. Khan, S. Khan, and M. Anwar, “A survey on smart grid technologies: Recent advances, challenges and future direction,” *IEEE Access*, vol. 9, pp. 69 752–69 799, 2021. [Online]. Available: <https://doi.org/10.1109/ACCESS.2021.3077890>
- [2] R. Kumar and H. Singh, “Iot-enabled smart energy systems: Architecture, applications, and challenges,” *Renewable and Sustainable Energy Reviews*, vol. 152, p. 111708, 2021. [Online]. Available: <https://doi.org/10.1016/j.rser.2021.111708>
- [3] A. Nourani and S. Khare, “Cybersecurity risks in iot-enabled ev charging infrastructures,” *Energy Informatics*, vol. 5, no. 1, p. 13, 2025. [Online]. Available: <https://doi.org/10.1186/s42162-025-00223-5>
- [4] P. Sharma and R. Sahu, “Time synchronization in iot networks: A comprehensive survey,” *Computer Networks*, vol. 181, p. 107447, 2020. [Online]. Available: <https://doi.org/10.1016/j.comnet.2020.107447>
- [5] W. Huang and M. Zhao, “Time synchronization vulnerabilities in smart grids: A modeling and analysis study,” *IEEE Transactions on Smart Grid*, vol. 13, no. 6, pp. 4880–4891, 2022. [Online]. Available: <https://doi.org/10.1109/TSG.2022.3174687>
- [6] V. Pieterse and M. Langerman, “Modeling oscillator drift in iot devices using stochastic processes,” *IEEE Internet of Things Journal*, vol. 8, no. 12, pp. 10 175–10 186, 2021. [Online]. Available: <https://doi.org/10.1109/IJOT2021.3056799>
- [7] C. Mendoza and R. Patel, “Characterizing timestamp jitter in low-cost iot sensors,” *Sensors*, vol. 23, no. 5, p. 2547, 2023. [Online]. Available: <https://doi.org/10.3390/s23052547>

[8] Inventive HQ Team, “The year 2038 problem: Understanding the next major time bug (y2038),” <https://inventivehq.com/blog/year-2038-problem-explained>, 2025, accessed: 2025-02-20.

[9] A. Aithal, A. Wainwright, and S. Atkins, “Interoperability of flexibility dispatch systems,” in *Distribution System Operation: Flexibility Services: Summary of Key Outputs From the Open Networks Programme*. Springer, 2025, pp. 149–180.

[10] R. Griffiths, “Time and the anthropocene: Making more-than-human temporalities legible through environmental observations and creative methods,” *Time & Society*, vol. 32, no. 4, pp. 461–487, 2023.

[11] A. McKenna and D. Rao, “Y2k38 and embedded system timekeeping vulnerabilities: Risks and mitigations,” *IEEE Embedded Systems Letters*, vol. 14, no. 3, pp. 158–162, 2022. [Online]. Available: <https://doi.org/10.1109/LES2022.3142165>

[12] D. Harris and P. Zhou, “Epoch overflow vulnerabilities in embedded linux systems: Experimental analysis,” *Journal of Systems Architecture*, vol. 145, p. 102896, 2024. [Online]. Available: <https://doi.org/10.1016/j.sysarc.2023.102896>

[13] D. Casciato, “Countdown to chaos: What you need to know about the unix time stamp problem in 2038,” Dev.to blog, 2023, accessed Feb. 20, 2025.

[14] H. Lee and J. Kim, “Analysis of ntp spoofing attacks in distributed cyber-physical systems,” *IEEE Transactions on Industrial Informatics*, vol. 19, no. 7, pp. 8450–8461, 2023. [Online]. Available: <https://doi.org/10.1109/TII.2023.3234567>

[15] F. Qureshi and Z. Ahmed, “Gps spoofing attacks on iot-based smart grids: Detection and mitigation,” *Electric Power Systems Research*, vol. 199, p. 107410, 2021. [Online]. Available: <https://doi.org/10.1016/j.epsr.2021.107410>

[16] S. Mehdi and N. Bouabdellah, “Lstm-based anomaly detection for industrial control systems: A survey,” *IEEE Access*, vol. 8, pp. 168 825–168 840, 2020. [Online]. Available: <https://doi.org/10.1109/ACCESS.2020.3022764>

[17] Y. Wang and J. Xu, “Gru-based predictive analytics for iot energy systems,” *Energy Reports*, vol. 7, pp. 5294–5303, 2021. [Online]. Available: <https://doi.org/10.1016/j.egyr.2021.08.153>

[18] L. Zhang and W. Song, “Graph neural networks for industrial iot security: A comprehensive review,” *ACM Computing Surveys*, vol. 55, no. 9, pp. 1–37, 2022. [Online]. Available: <https://doi.org/10.1145/3527153>

[19] S. Alipour and M. Faraj, “Spatio-temporal graph neural networks for anomaly detection in cyber-physical systems,” in *2023 ACM/IEEE International Conference on Cyber-Physical Systems (ICCPs)*, 2023, pp. 143–154. [Online]. Available: <https://doi.org/10.1109/ICCPs56610.2023.00022>

[20] H. Yiğitler, J. Lehtomäki, O. Özdemir, and M. Özger, “Overview of time synchronization for iot deployments,” *Sensors*, vol. 20, no. 18, pp. 1–33, 2020. [Online]. Available: <https://doi.org/10.3390/s20185160>

[21] K.-B. Liu, Y. Li, C. Wang *et al.*, “A survey on clock synchronization in the industrial internet,” *Journal of Computer Science and Technology*, vol. 38, no. 3, pp. 553–574, 2023. [Online]. Available: <https://doi.org/10.1007/s11390-023-2453-3>

[22] Y. Liu, H. Zhang, Y. Cao, and S. Su, “Time synchronization techniques in the modern smart grid: Requirements, challenges, and future trends,” *Energies*, vol. 18, no. x, pp. 1–24, 2025, online first. [Online]. Available: <https://www.mdpi.com/energies>

[23] H. Zhang, S. Peng, L. Liu, S. Su, and Y. Cao, “Review on GPS spoofing-based time synchronisation attack on power system,” *IET Generation, Transmission & Distribution*, vol. 14, no. 20, pp. 4301–4309, 2020. [Online]. Available: <https://doi.org/10.1049/iet-gtd.2020.0253>

[24] A. Xue, X. Wang, Y. Zhang *et al.*, “Data-driven detection for GPS spoofing attack using phasor measurement units,” *International Journal of Electrical Power & Energy Systems*, vol. 129, p. 106787, 2021. [Online]. Available: <https://doi.org/10.1016/j.ijepes.2021.106787>

[25] I. Khan, M. Netto, and M. Kezunovic, “Undetectable relentless incremental GPS-spoofing attack on time series PMU data,” *IEEE Transactions on Smart Grid*, vol. 13, no. 6, pp. 4891–4903, 2022. [Online]. Available: <https://doi.org/10.1109/TSG.2022.3174605>

[26] Y. Liu, X. Chen, F. Wang *et al.*, “Detection and mitigation of time synchronization attacks in smart grids using LSTM-based forecasting,” *Electric Power Systems Research*, vol. 228, p. 110132, 2024. [Online]. Available: <https://doi.org/10.1016/j.epsr.2024.110132>

[27] M. Sabouri, S. Siamak, M. Dehghani, and V. Peric, “Increasing the resiliency of power systems in presence of GPS spoofing attacks: A data-driven deep-learning algorithm,” *IET Generation, Transmission & Distribution*, vol. 17, no. 9, pp. 1861–1873, 2023. [Online]. Available: <https://doi.org/10.1049/gtd2.12713>

[28] K. Ou, J. Wang, and X. Li, “Time synchronization attack protection scheme based on multi-source time fusion for GNSS-dependent power systems,” *Electronics*, vol. 14, no. x, pp. 1–18, 2025. [Online]. Available: <https://www.mdpi.com/journal/electronics>

[29] X. Jia, P. Xun, W. Peng, B. Zhao, H. Li, and C. Shen, “Deep anomaly detection for time series: A survey,” *Computer Science Review*, vol. 58, p. 100787, 2025. [Online]. Available: <https://doi.org/10.1016/j.cosrev.2025.100787>

[30] J. Backhus, A. R. Rao, C. Venkatraman, and C. Gupta, “Time series anomaly detection using signal processing and deep learning,” *Applied Sciences*, vol. 15, no. 11, p. 6254, 2025. [Online]. Available: <https://doi.org/10.3390/app15116254>

[31] X. Liu, S. Yin, J. Wang, J. Zhu, X. Wang, and Y.-H. Yang, “Rtdetector: Deep transformer networks for time series anomaly detection based on reconstruction trend,” in *Proceedings of the 34th International Joint Conference on Artificial Intelligence (IJCAI)*, 2025, pp. 5766–5774. [Online]. Available: <https://doi.org/10.24963/ijcai.2025/644>

[32] Y. Zheng, H. Y. Koh, M. Jin, L. Chi, H. Wang, K. T. Phan, Y.-P. P. Chen, S. Pan, and W. Xiang, “Graph spatiotemporal process for multivariate time series anomaly detection with missing values,” *Information Fusion*, vol. 106, p. 102255, 2024. [Online]. Available: <https://doi.org/10.1016/j.inffus.2024.102255>

[33] Y. Di, F. Wang, Z. Zhao, Z. Zhai, and X. Chen, “An interpretable graph neural network for real-world satellite power system anomaly detection based on graph filtering,” *Expert Systems with Applications*, vol. 254, p. 124348, 2024. [Online]. Available: <https://doi.org/10.1016/j.eswa.2024.124348>

[34] C. Lu, Z. Yu, F. Qian, D. Shang, T. Chen, J. Luo, X. Hui, and H. Li, “Heterogeneous data fusion and anomaly detection in industrial IoT systems using spatio-temporal graph neural networks,” in *Proceedings of the 2024 4th International Symposium on Artificial Intelligence and Intelligent Manufacturing (AIIM)*, 2024, pp. 548–556. [Online]. Available: <https://doi.org/10.1109/AIIM64537.2024.10934344>

[35] Y. AlZahrani *et al.*, “Real-time anomaly detection in IoT streams through deep learning-based feature extraction,” *Discover Internet of Things*, vol. 5, no. x, pp. 1–19, 2025. [Online]. Available: <https://doi.org/10.1007/s43926-025-00256-9>

[36] H. N. Zaky, M. G. Abd Elfatah, S. A. El-Mongy, and M. A. Abdel-Rahman, “Euler–maruyama algorithm in estimating ugv path and location in nuclear emergency and security applications,” *Kerntechnik*, vol. 88, no. 3, pp. 361–369, 2023.

[37] N. Thrimoorthy, R. Chandramma, S. Unnikrishnan, and K. Vanitha, “Ornstein uhlenbeck cache obliviousness neural congestion control in wireless network for iot data transmission,” *Int. J. Comput. Netw. Appl.*, vol. 10, no. 1, 2023.

[38] T. Kailath and J. Chun, “Generalized displacement structure for block-toeplitz, toeplitz-block, and toeplitz-derived matrices,” *SIAM Journal on Matrix Analysis and Applications*, vol. 15, no. 1, pp. 114–128, 1994.

[39] D. A. Knoll and D. E. Keyes, “Jacobian-free newton–krylov methods: a survey of approaches and applications,” *Journal of Computational Physics*, vol. 193, no. 2, pp. 357–397, 2004.

[40] S. Pradhan, “Edge-iiotset dataset,” Kaggle: Datasets, 2023, available: <https://www.kaggle.com/datasets/sibasispradhan/edge-iiotset-dataset>. [Online]. Available: <https://www.kaggle.com/datasets/sibasispradhan/edge-iiotset-dataset>

[41] T. Sakai, “Two sample t-tests for ir evaluation: Student or welch?” in *Proceedings of the 39th International ACM SIGIR conference on Research and Development in Information Retrieval*, 2016, pp. 1045–1048.

[42] J.-C. Goulet-Pelletier and D. Cousineau, “A review of effect sizes and their confidence intervals, part i: The cohen’sd family,” *The Quantitative Methods for Psychology*, vol. 14, no. 4, pp. 242–265, 2018.

[43] H. Zhao, L. Yin, Z. Wu, Q. Wei, L. Song, and S. Yang, “Multivariate time-series anomaly detection via graph attention networks,” pp. 908–917, 2020.

[44] A. Deng and B. Hooi, “Graph deviation network for multivariate time series anomaly detection,” in *Proceedings of the 30th ACM International Conference on Information and Knowledge Management*. ACM, 2021, pp. 2321–2330.

[45] D. Xu, H. Wang, Y. Chen, K. Zha, W. Hu, J. Sun, Z. Liu, Q. Wu, and B. Ding, “Anomaly transformer: Time series anomaly detection with association discrepancy,” in *Proceedings of the 35th Conference on Neural Information Processing Systems (NeurIPS)*, 2021.

[46] S. Chen, J. Jiang, L. Chen, and J. Chen, “Gta: Graph-transformer architecture for multivariate time series anomaly detection in iot,” *IEEE Internet of Things Journal*, vol. 8, no. 8, pp. 6300–6310, 2021.

[47] X. Liu, X. Zhu, J. Yang, and L. Wen, “Sarad: Self-attention reconstruction for anomaly detection in multivariate time series,” *Information Sciences*, vol. 630, pp. 436–451, 2023.